

# Image reconstruction for 2D homogeneous dielectric cylinder using FDTD method and SSGA

Wei Chien<sup>a</sup>, Chung-Hsin Huang<sup>b</sup>, Chien-Ching Chiu<sup>b,\*</sup> and Ching-Lieh Li<sup>b</sup>

<sup>a</sup>*Electronic Engineering Department, De Lin Institute of Technology, Tu-Cheng, Taipei, Taiwan*

<sup>b</sup>*Electrical Engineering Department, Tamkang University, Tamsui, Taiwan*

**Abstract.** This paper presents an image reconstruction approach for a 2-D homogeneous cylinder with arbitrary cross section in free space. The computational method combines the finite difference time domain (FDTD) method and non-uniform steady state genetic algorithm (NU-SSGA) to determine the shape and location of the scatterer with arbitrary shape. The subgridding technique is implemented for modeling the shape of the cylinder more closely. The inverse problem is reformulated into an optimization problem and the global searching scheme NU-SSGA with closed cubic-spline is then employed to search the parameter space. A set of representative numerical results is presented for demonstrating that the proposed approach is able to efficiently reconstruct the electromagnetic properties of homogeneous dielectric scatterer even when the initial guess is far away from the exact one. In addition, the effects of Gaussian noises on imaging reconstruction are also investigated.

Keywords: Index terms – time domain inverse scattering, microwave imaging, FDTD, subgridding FDTD, NU-SSGA

## 1. Introduction

Inverse scattering comprises of wide spectrum of applications, such as non-destructive problem, medical imaging, geophysical prospecting, where the scattering object with unknown electromagnetic properties are reconstructed by scattered field excited by known set of sources. The most important mathematical characteristic of inverse problems is that they are ill-posed [1]. That means that large changes in the EM properties of object can produce very small changes in the scattered data. In general, the ill-posed problem can be treated by regularization schemes or transformed into a better conditioned problem [2].

Alternatively, the fact that the inverse problem is nonlinear is due to the dependence of scattering fields upon the electromagnetic properties of scatterer and total field in the scatterer domain simultaneously. The nonlinearity of the problem is treated and resolved by using iterative optimization techniques. As a result, many inverse problems are reformulated into optimization ones and then resolved by different iterative methods which can be briefly categorized as: local inversion approaches and global inversion approaches. Most of local inversion approaches employ the gradient-based searching scheme to find the extreme of the cost function, such as Newton-Kantorovitch method [3,4] and Levenberg-Marquardt algorithm [5], etc. However, these approaches are highly dependent on the initial guess and usually

---

\*Corresponding author. E-mail: chiu@ee.tku.edu.tw.

get trapped in the local extreme. Thus, some global inversion approaches are proposed to overcome the drawbacks of these local inversion ones. The global inversion approaches, including the genetic algorithms (GAs) [6,7], differential evolution (DE) [8,9], particle swarm optimization (PSO) [10,11] and Ant colony optimization (ACO) [12], are in general stochastic, adaptive searching algorithm. The GAs [13] is an evolutionary algorithm that uses the stochastic mechanism to search through the parameter space. As compared to the gradient-based searching techniques, the genetic algorithm is less prone to converge to a local extreme. In past years, most of researchers applied GAs together with frequency domain electromagnetic solver to attack the inverse scattering problem [14–16]. Fewer researchers had applied the genetic/evolutionary algorithms in the time domain inverse scattering problem for metallic target identification [17,18] and penetrable object reconstruction [19,20]. To the best of our knowledge, there is still no investigation on using the GA to reconstruct the location, shape function and permittivity of homogeneous dielectric cylinders imaging problem in free space under time domain.

This paper presents a time domain computational scheme for the microwave imaging of a 2D homogeneous dielectric cylinder with arbitrary cross section in free space. The forward problem is solved based on the FDTD method, for which the subgridding technique is implemented to closely describe the fine structure of the cylinder [21]. Interpolation technique through the closed cubic B-splines [22] is employed to describe a cylinder with arbitrary shape more effectively instead of the frequently used trigonometric series expansion. The inverse problem is formulated into an optimization one and then the non-uniform steady state genetic algorithm (NU-SSGA) [23] previously published by the authors is used to search the parameter space.

In session II, the subgridding FDTD method for the forward scattering are presented. In session III, the numerical results of the proposed inverse problem are given. Finally, in session IV some conclusions are drawn for the proposed time domain inverse scattering.

## 2. Forward problem

Consider a homogeneous dielectric cylinder located in free space as depicted in Fig. 1. The cross section of the object is starlike shape that can be representation in polar coordinates in the x-y plane with respect to the center position  $(X_O, Y_O)$ . The permittivity and permeability of free space and dielectric object are denoted by  $(\varepsilon_0, \mu_0)$  and  $(\varepsilon_2, \mu_2)$ , respectively. The dielectric object is illuminated by Gaussian pulse line source located at the points denote by Tx and scattered waves are recorded at those points denoted by Rx. The computational domain is discretized by the Yee's cell. It should be mentioned that the computational domain is surrounded by the optimized PML absorber [24] to reduce the reflection from the air-PML interface.

### 2.1. Cubic spline interpolation technique

The local shape function  $F(\theta)$  of the scatterer is approximated by the closed cubic B-splines for the sake of reducing the unknowns required to describe the arbitrary shape more effectively. As shown in Fig. 2, The boundary of the shape of the scatterer could be separated into  $N$  pieces which consist of the polynomials of degree 3  $P_i(\theta)$ ,  $i = 1, 2, \dots, N$  and have separated  $N + 1$  points. The closed cubic spline, which satisfy the following smooth conditions:

$$\begin{aligned} P_i(\theta_i) &= P_{i+1}(\theta_i) = \rho_i \\ P'_i(\theta_i) &= P'_{i+1}(\theta_i) \\ P''_i(\theta_i) &= P''_{i+1}(\theta_i) \end{aligned} \quad i = 1, 2, \dots, N \quad (1)$$

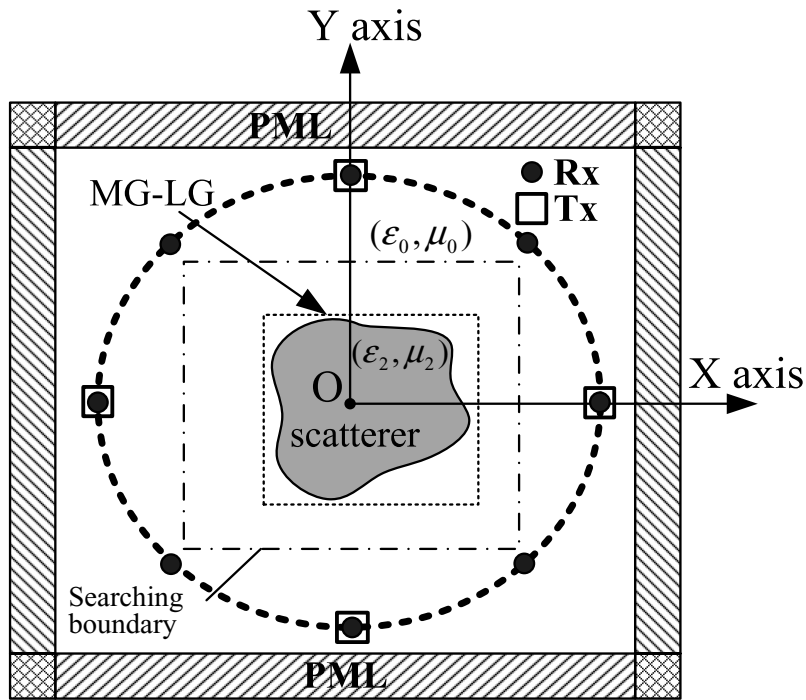


Fig. 1. Geometrical configuration for the inverse scattering.

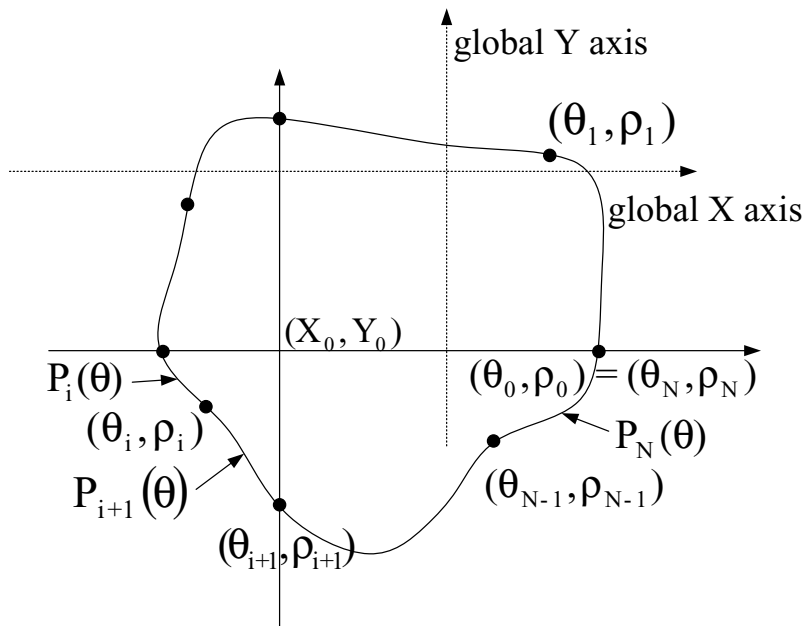


Fig. 2. Geometry of the cubic-spline.  $(\theta_i, \rho_i)$  is the polarized-coordinate expression for each point and  $P_i(\theta)$  is the function of the cubic line which links the points  $(\theta_{i-1}, \rho_{i-1})$  and  $(\theta_i, \rho_i)$ .

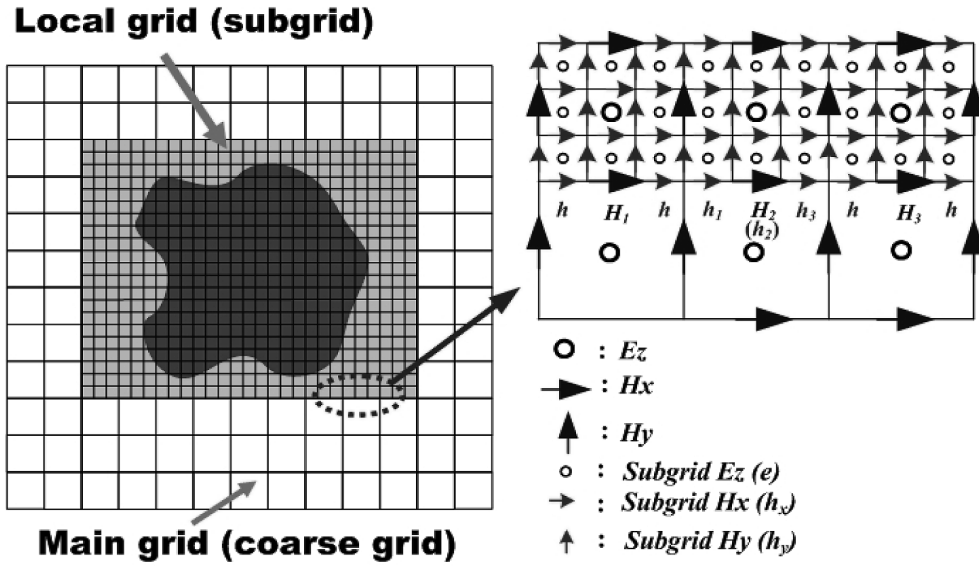


Fig. 3. The structure of the  $TM_z$  FDTD major grids and local grids for the scaling ratio (1:3): H fields are aligned with the MG-LG boundary.

and

$$\begin{aligned}
 P_1(\theta_0) &= P_N(\theta_N) \\
 P_1'(\theta_0) &= P_N'(\theta_N) = \rho_N' \\
 P_1''(\theta_0) &= P_N''(\theta_N)
 \end{aligned}
 \tag{2}$$

Through the interpolation of the cubic spline, an arbitrary smooth cylinder can be easily described through a few parameters  $\rho_1, \rho_2, \dots, \rho_N$  and the slope [22]. In order to closely describe the shape of the cylinder for the forward scattering procedure, the subgridding technique is implemented in the FDTD code, the details are presented as follows.

### 2.2. Subgrid FDTD

A subgridding scheme is employed to divide the problem space into regions with different grid sizes. The grid size in coarse region is about  $(\frac{1}{20} \sim \frac{1}{10} \lambda_{\max})$  as in normal FDTD, while in the fine region the grid size is scaled by an integer ratio. As an example, the Yee cells with subgridding structure are shown in Fig. 3, of which the scaling ratio is 1:3. For the time domain scattering and/or inverse scattering problem, the scatterers can be assigned with the fine region such that the fine structure can be easily described. If higher resolution is needed, only the fine region needs to be rescaled using a higher ratio for subgridding. This can avoid gridding the whole problem space using the finest resolution such that the computational resources are utilized in a more efficient way, which is quite important for the computational intensive inverse scattering problems.

In Fig. 3,  $E$  and  $H$  stand for the electric and magnetic fields on the major grids, respectively, while  $e$  and  $h$  denote the fields on the local grids. If the scaling ratio is set at odd-ratio, for example 1:3, then the  $E$  and  $H$  fields coincide with  $e$  and fields in the fine region.

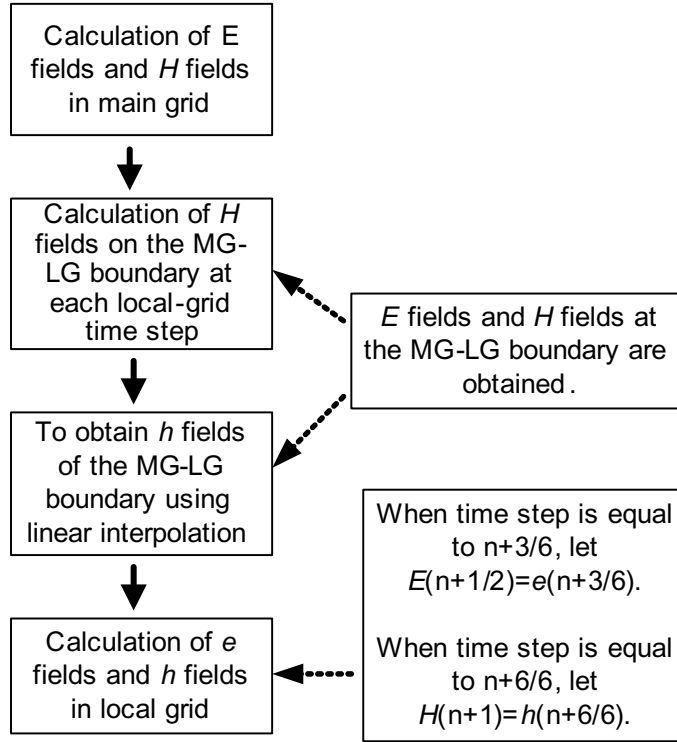


Fig. 4. Flowchart to update the (E, H) fields on the major grids and (e, h) fields on local grids.

Since the local grid size is one third of the main grid size, the time stepping interval  $\Delta t'$  for the  $e$  and  $h$  fields on the local grids is also one third of that for the  $E$  and  $H$  fields on the main grids.

Note that the  $e$  and fields inside the fine region can be updated through the normal Yee-cell algorithm except those at the MG-LG boundary, such as  $h_1$ ,  $h_2$  and  $h_3$ , for example.

The  $h$  fields at the MG-LG interface can be linearly interpolated as follows:

$$\begin{aligned}
 h_1^{n+v} &= H_1^{n+v} + \frac{2}{3} (H_2^{n+v} - H_1^{n+v}) \\
 h_2^{n+v} &= H_2^{n+v}, \quad \text{for } v = \frac{1}{3}, \frac{2}{3} \text{ and } \frac{3}{3}. \\
 h_3^{n+v} &= H_2^{n+v} + \frac{1}{3} (H_3^{n+v} - H_2^{n+v})
 \end{aligned} \tag{3}$$

Note that for Eq. (3) the  $H^{n+v}$  fields don't exist on the main grids actually for  $v = \frac{1}{3}$  and  $\frac{2}{3}$  and need extra parabolic interpolation calculation by

$$H^{n+v} = H^n + Av + \frac{Bv^2}{2} \tag{4}$$

with  $A = \frac{H^{n+1} - H^{n-1}}{2}$

$$B = H^{n+1} - H^{n-1} - 2H^n$$

The flow chart associated to update the fields in the fine region is shown in Fig. 4. Note that at the time step  $n + \frac{3}{6}$  the  $E^{n+\frac{3}{6}}$  fields on the main grids should be updated by the coincided  $e^{n+\frac{3}{6}}$  fields on the local grids. Similarly, at the time step  $n + \frac{6}{6}$  the  $H^{n+1}$  fields are updated by the coincided  $h^{n+\frac{6}{6}}$  fields.

### 3. Inverse problem

For the inverse scattering problem, the shape, location and permittivity of the dielectric cylinder are reconstructed by the given scattered electric field obtained at the receivers. This problem is resolved by an optimization approach, for which the global searching scheme NU-SSGA previously reported by the author [16] is employed to minimize the following fitness:

$$OF = \frac{\sum_{n=1}^{N_i} \sum_{m=1}^M \sum_{s=0}^S |E_z^{exp}(n, m, s\Delta t) - E_z^{cal}(n, m, s\Delta t)|}{\sum_{n=1}^{N_i} \sum_{m=1}^M \sum_{s=0}^S |E_z^{exp}(n, m, s\Delta t)|} \quad (5)$$

where  $E_z^{exp}$  and  $E_z^{cal}$  are experimental electric fields and the calculated electric fields, respectively. The  $N_i$  and  $M$  are the total number of the transmitters and receivers, respectively.  $S$  is the total time step number of the recorded electric fields.

The genetic algorithms are very powerful stochastic global optimization methods based on genetic recombination and evaluation in nature [18]. GAs have been widely applied to the global numerical optimization problem in field of science and engineering. In general, a typical GAs optimizer must be able to perform seven basic tasks:

1. Encode the solution parameters as genes,
2. Create a string of the genes to form a chromosome,
3. Initialize a starting population,
4. Evaluate and assign fitness values to individuals in the population,
5. Perform reproduction through some selection scheme,
6. Perform recombination of genes to produce offspring, and
7. Perform mutation of genes to produce offspring.

The key distinction between an NU-SSGA and a typical GAs is on the number of fitness calculation. In a typical GAs, each generation of the algorithm replaces the population with the new population. On the contrary, NU-SSGA only needs to generate a few offspring, by non-uniform beta distribution in crossover and mutation, to replace the weakest individual in each new generation. The non-uniform probability density scheme in genetic operator could increase the searching diversity in the early iteration, and also increase the exploration ability of the algorithm in latter iteration. In other words, the number of fitness calculation corresponding to the new population is large in a typical GA compared with NU-SSGA. To prevent the superior individual from being lost during the GA optimization process, the rank scheme is employed in the selection operation for which copies the superior individual to the next generation. Based on the characteristic of NU-SSGA in reducing the numbers of fitness calculation, we are able to reconstruct the microwave image efficiently.

#### 4. Numerical results

In this section, we report some numerical results using the method described in Section 2. As shown in Fig. 1, the problem space is divided in  $68 \times 68$  grids with the grid size  $\Delta x = \Delta y = 5.95$  mm. The homogeneous dielectric cylinder is located in free space. The cylindrical object is illuminated by a transmitter at four different positions,  $N_i = 4$ . The scattered  $E$  fields for each illumination are collected at the eight receivers,  $M = 8$ . Note that the simulated result using one incident wave is much worse than that by two incident waves. In order to get better result, four transmitters are used here. The transmitters and receivers are collocated at a distance of 24 grids from the origin. The incident current pulse  $I_z(t)$  is expressed as:

$$I_z(t) = \begin{cases} Ae^{-\alpha(t-\beta\Delta t)^2} & , t \leq T_w \\ 0 & , t > T_w \end{cases} \quad (6)$$

where  $\beta = 24$ ,  $A = 1000$ ,  $\Delta t = 13.34$  ps,  $T_w = 2\beta\Delta t$ , and  $\alpha = \left(\frac{1}{4\beta\Delta t}\right)^2$

The time duration is set to  $250 \Delta t$  ( $S = 250$ ). Note that in order to accurately describe the shape of the cylinder, the subgridding FDTD technique is used both in the forward scattering (1:9) and the inverse scattering (1:5) parts – but with different scaling ratios as indicated in the parentheses. For the forward scattering, the  $E$  fields generated by the FDTD with fine subgrids are used to mimic the experimental data in Eq. (5).

Three examples are investigated for the inverse scattering of the proposed structure by using NU-SSGA. There are twelve unknown parameters to retrieve, which include the center position ( $X_O, Y_O$ ), the radius  $\rho_i$ ,  $i = 1, 2, \dots, 8$  of the shape function and the slope  $\rho'_N$  plus the relative permittivity of the object,  $\varepsilon_r = \varepsilon_2/\varepsilon_0$ . Very wide searching ranges are used for the NU-SSGA to optimize the const function given by Eq. (5). The parameters and the corresponding searching ranges are listed follows:  $-47.6 \text{ mm} \leq X_O \leq 47.6 \text{ mm}$ ,  $-47.6 \text{ mm} \leq Y_O \leq 47.6 \text{ mm}$ ,  $0 \text{ mm} \leq \rho_i \leq 59.5 \text{ mm}$ ,  $i = 1, 2, \dots, 8$ ,  $-1 \leq \rho'_N \leq 1$  and  $1 \leq \varepsilon_r \leq 16$ . The relative coefficients of the NU-SSGA are set as below: The crossover rate and the mutation rate are set to 0.1 and 0.05, respectively. The population size set 144 and the rank is set to 108.

The first example, the dielectric cylinder with the shape function of the unknown scatterer is selected by the cubic-spline expansion to be  $\rho_1 = 35.7$  mm,  $\rho_2 = 35.7.16$  mm,  $\rho_3 = 23.8$  mm,  $\rho_4 = 23.8$  mm,  $\rho_5 = 35.7$  mm,  $\rho_6 = 35.7$  mm,  $\rho_7 = 29.75$  mm,  $\rho_8 = 29.75$  mm, and slope is 0. The relative permittivity  $\varepsilon_r$  of this dielectric object is 3.4. The reconstructed shape function of the best individual is plotted in Fig. 5 for different generations. The r.m.s. error (DF) of the reconstructed shape  $F^{cal}(\theta)$  and the relative error (DIPE) of  $\varepsilon_r^{cal}$  with respect to the exact values versus generation are shown in Fig. 6. Here, DF and DIPE are defined as

$$DF = \left\{ \frac{1}{N'} \sum_{i=1}^{N'} [F^{cal}(\theta_i) - F(\theta_i)]^2 / F^2(\theta_i) \right\}^{1/2} \quad (7)$$

$$DIPE = \frac{|\varepsilon_r^{cal} - \varepsilon_r|}{\varepsilon_r} \quad (8)$$

where the  $N'$  is set to 160. The r.m.s. error DF is about 3.6% and DIPE = 1.5%. It is seen that the reconstruction is good.

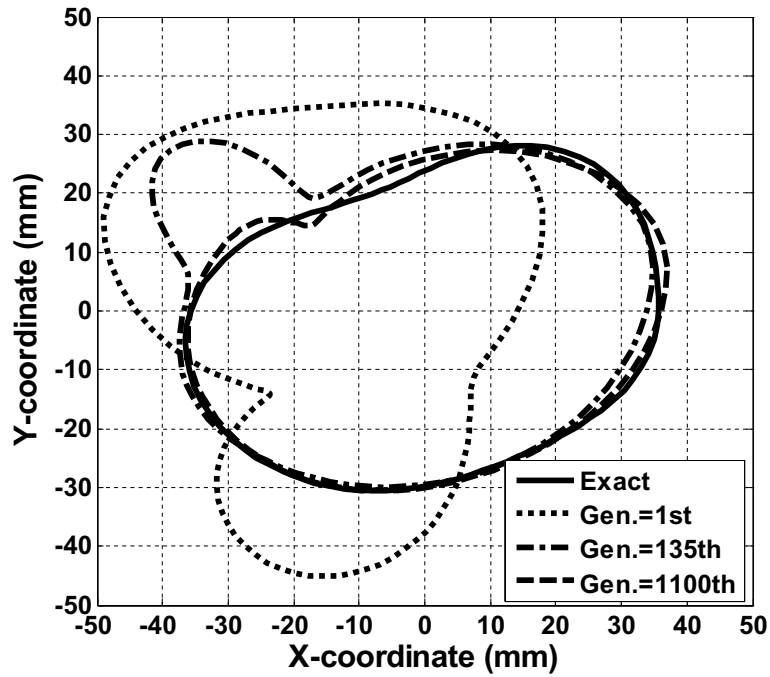


Fig. 5. The reconstructed shape of the cylinder at different generations for example 1.

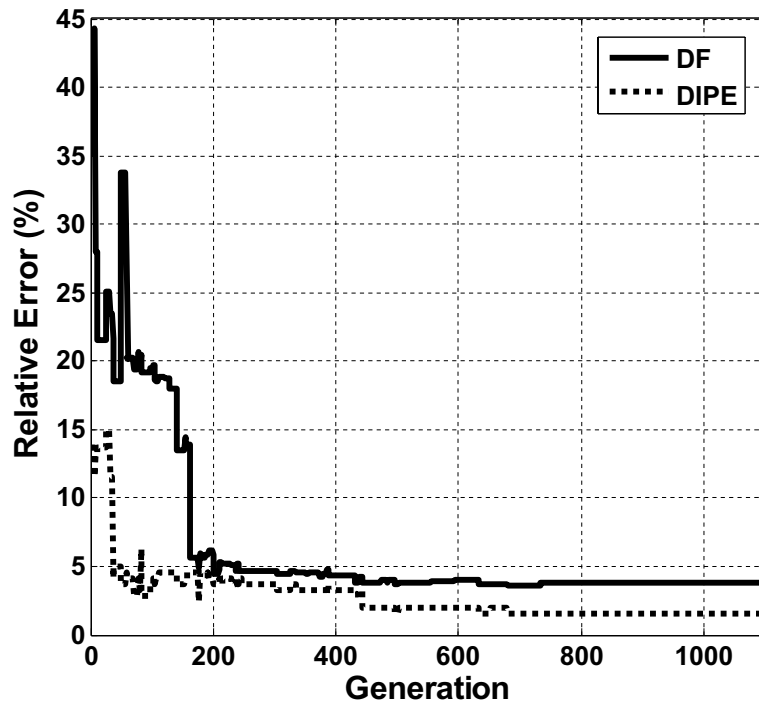


Fig. 6. Shape function error and permittivity error at each generation of example 1.

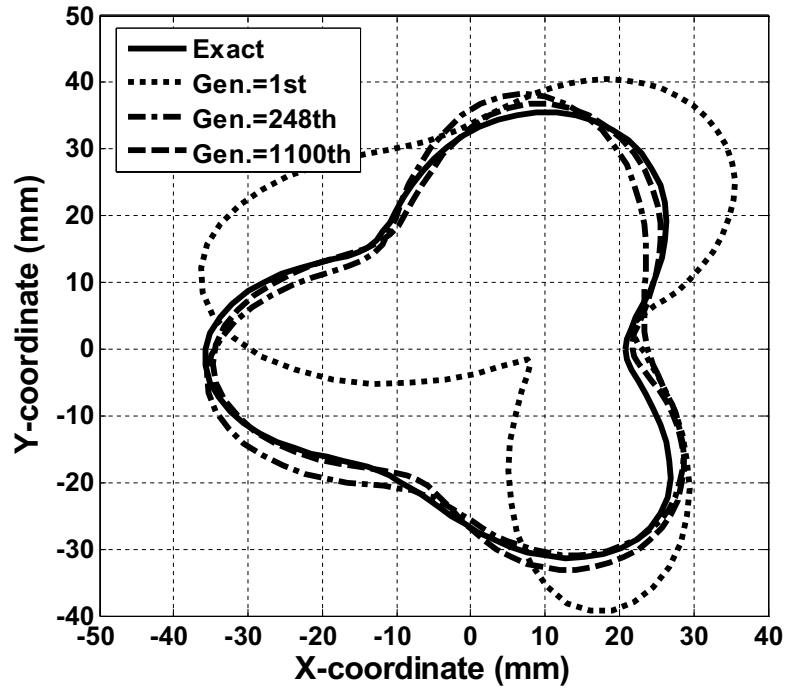


Fig. 7. The reconstructed cross section of the cylinder of example 2 at different generations.

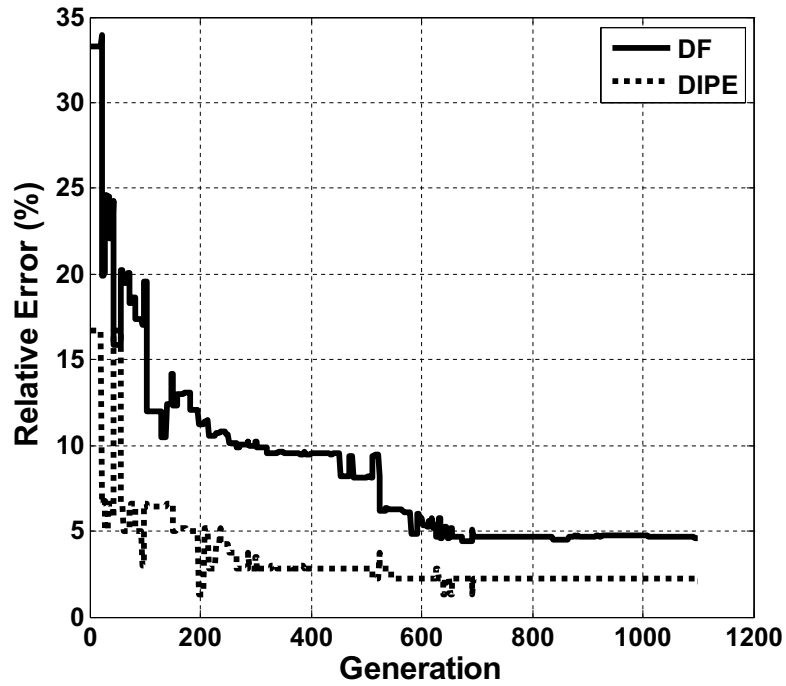


Fig. 8. Shape function error and permittivity error for different generations of example 2.

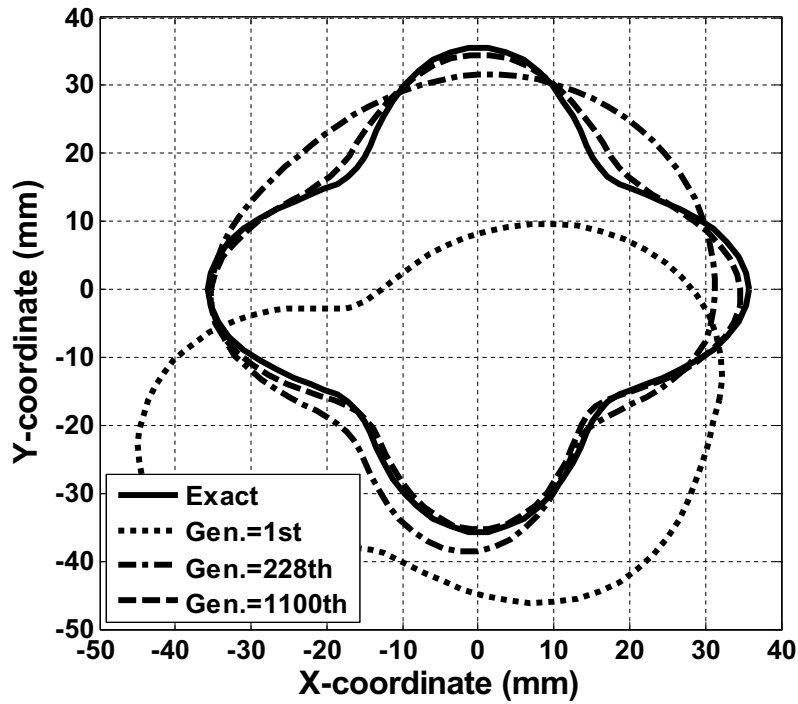


Fig. 9. The reconstructed cross section of the cylinder of example 3 at sequential generations.

In the second example, the shape function of dielectric cylinder is selected to be  $\rho_1 = 20.825$  mm,  $\rho_2 = 35.7$  mm,  $\rho_3 = 32.725$  mm,  $\rho_4 = 20.825$  mm,  $\rho_5 = 35.7$  mm,  $\rho_6 = 23.8$  mm,  $\rho_7 = 26.775$  mm,  $\rho_8 = 35.7$  mm, and slope is 0. The relative permittivity  $\epsilon_r$  of this dielectric object is 7.7. This example is to demonstrate the capability of the proposed method to reconstruct a dielectric cylinder with high-contrast permittivity. The reconstructed images for different generations and the relative error of this object are shown in Figs 7 and 8, respectively. The r.m.s. error DF is about 4.6% and DIPE = 2.1% in the final generation. From the reconstructed result of this object, we conclude the proposed method can be used to reconstruct dielectric cylinder successfully when the dielectric object is with high-contrast permittivity. The above two examples show that the permittivity converges fast than the shape function to the corresponding exact values.

The reconstructed result of the final example is shown in Fig. 9, where the shape is  $\rho_1 = 35.7$  mm,  $\rho_2 = 23.8$  mm,  $\rho_3 = 35.7$  mm,  $\rho_4 = 23.8$  mm,  $\rho_5 = 35.7$  mm,  $\rho_6 = 23.8$  mm,  $\rho_7 = 35.7$  mm,  $\rho_8 = 23.8$  mm, and slope is 0. The relative permittivity  $\epsilon_r$  of this dielectric object is 3.2. Figure 10 shows that the relative errors of the shape and the permittivity decrease quickly by generations. The r.m.s. error DF is about 3.8% and DIPE = 0.8%. In order to investigate the sensitivity of the imaging algorithm against the random noise, the additive white Gaussian noise of zero mean is added into the experimental electric fields. Normalize standard deviations of  $10^{-4}$ ,  $10^{-3}$ ,  $10^{-2}$ ,  $10^{-1}$ , 0.2 and 0.5 are used. The normalized standard deviation mentioned earlier is defined as the standard deviation of the Gaussian noise divided by the r.m.s. value of the scattered fields. Figure 11 shows the reconstructed results under the condition that the experimental scattered field is contaminated by the noise. It could be observed that good reconstruction has been obtained for both the relative permittivity and shape of the dielectric cylinder when the normalize standard deviations is below  $10^{-1}$ .

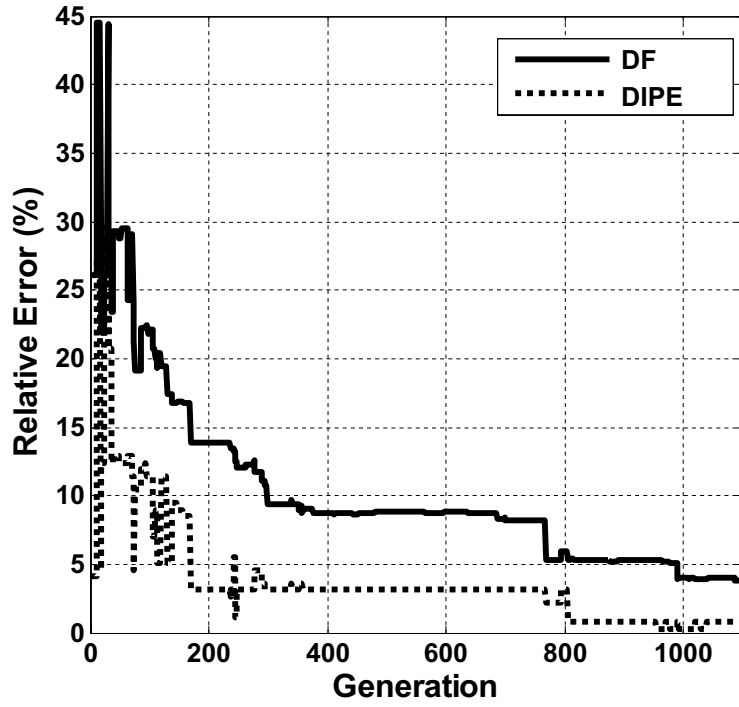


Fig. 10. Shape function error and permittivity error at different generations of example 3.

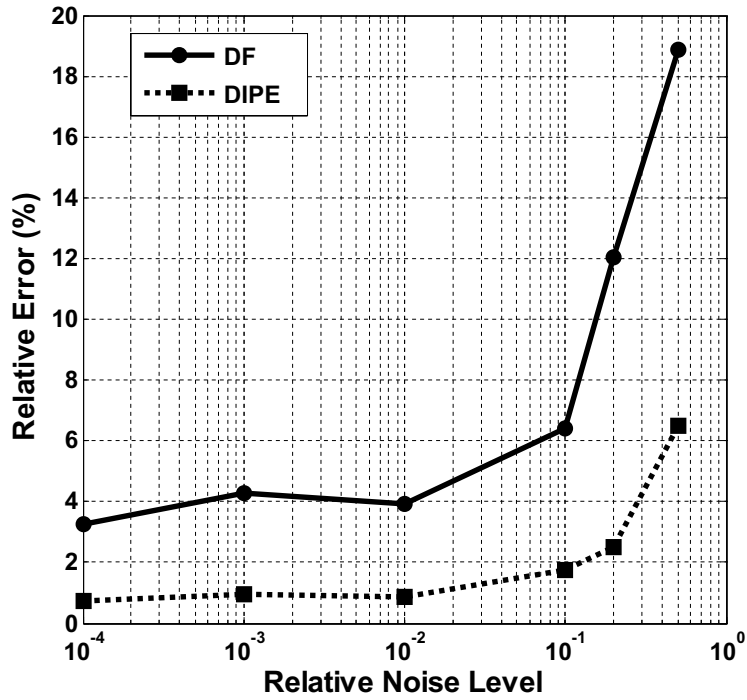


Fig. 11. Shape error as functions of noise for the final example.

## 5. Conclusion

In this paper, a computational approach to microwave imaging of homogeneous dielectric scatterer with arbitrary cross section in time domain has been presented. Scattering fields are obtained by FDTD method. The subgridding scheme is employed to closely describe the shape of the cylinder for the FDTD method. The approach has been formulated as a global nonlinear optimization problem and NU-SSGA has been applied. It has been shown that the location, shape and permittivity of the dielectric object can be successfully reconstructed even when the dielectric object with fairly large permittivity and the Born approximation is no longer valid. In our study, good reconstructed results are obtained even when the initial guess is far from the exact one, while the gradient-based methods often get stuck in a local extreme. Numerical results have been carried out and good reconstruction has been obtained even in the presence of white Gaussian noise in experimental data.

## References

- [1] D. Colton and R. Kress, *Inverse Acoustic and Electromagnetic Scattering Theory*, Springer-Verlag, New York, 1992.
- [2] H.W. Engl, M. Hanke and A. Neubauer, *Regularization of Inverse Problems*, Kluwer Academic Publishers, Dordrecht, 2000.
- [3] C.C. Chiu and Y.W. Kiang, Microwave imaging of multiple conducting cylinders, *IEEE Transactions on Antennas and Propagation* **40**(8) (August 1992), 933–941.
- [4] A. Roger, Newton-Kantorovitch algorithm applied to an electromagnetic inverse problem, *IEEE Transactions on Antennas and Propagation* **29** (March 1981), 232–238.
- [5] A. Francois and C. Pichot, Microwave imaging: Complex permittivity reconstruction with a Levenberg-Marquardt method, *IEEE Transactions on Antennas and Propagation* **45** (1997), 203–215.
- [6] C.H. Huang, Y.F. Chen and C.C. Chiu, “Permittivity distribution reconstruction of dielectric objects by a cascaded method,” *Journal of Electromagnetic Waves & Applications* **21**(2) (2007), 145–159.
- [7] S. Caorsi, A. Massa and M. Pastorino, A computational technique based on a real-coded genetic algorithm for microwave imaging purposes, *IEEE Transactions on Geoscience and Remote Sensing* **38**(4) (July 2000), 1697–1708.
- [8] K.A. Michalski, Electromagnetic imaging of circular-cylindrical conductors and tunnels using a differential evolution algorithm, *Microwave and Optical Technology Letters* **27**(5) (Dec 2000), 330–334.
- [9] A. Qing, Electromagnetic inverse scattering of multiple two-dimensional perfectly conducting objects by the differential evolution strategy, *IEEE Transactions on Antennas and Propagation* **51**(6) (2003), 1251–1262.
- [10] M. Donelli and A. Massa, Computational approach based on a particle swarm optimizer for microwave imaging of two-dimensional dielectric scatterers, *IEEE Transactions on Microwave Theory and Techniques* **53**(5) (May 2005), 1761–1776.
- [11] T. Huang and A.S. Mohan, Application of particle swarm optimization for microwave imaging of lossy dielectric objects, *IEEE Antenna and Propagation Society International Symposium Digest* (2005), 852–855.
- [12] M. Pastorino, Stochastic Optimization Methods Applied to Microwave Imaging: A Review, *IEEE Transactions on Antennas and Propagation* **55**(3) (March 2007), 538–548.
- [13] D.E. Goldberg, *Genetic Algorithm in Search, Optimization and Machine Learning*, Addison-Wesley, 1989.
- [14] A. Qing, An experimental study on electromagnetic inverse scattering of a perfectly conducting cylinder by using the real-coded genetic algorithm, *Microwave and Optical Technology Letters* **30** (September 2001), 315–320.
- [15] T. Takenaka, Z.Q. Meng, T. Tanaka and W. C. Chew, Local shape function combined with genetic algorithm applied to inverse scattering for strips, *Microwave and Optical Technology Letters* **16** (December 1997), 337–341.
- [16] C.L. Li, S.H. Chen, C.M. Yang and C.C. Chiu, Image reconstruction for a partially immersed perfectly conducting cylinder using the steady state genetic algorithm, *Radio Sci* **39**, RS2016, doi:10.1029/2002RS002742, 2004.
- [17] X.-M. Zhong, C. Liao and W. Chen, Image reconstruction of arbitrary cross section conducting cylinder using UWB pulse, *Journal of Electromagnetic Waves Application* **21**(1) (2007), 25–34.
- [18] C.H. Huang, C.C. Chiu, C.L. Li and Y.H. Li, Image Reconstruction of the Buried Metallic Cylinder Using FDTD Method and SSGA, *Progress In Electromagnetics Research* **PIER 85** (2008), 195–210.
- [19] X. Chen and K. Huang, Microwave Imaging of buried inhomogeneous objects using parallel genetic algorithm combined with FDTD method, *Progress In Electromagnetics Research* **PIER 53** (2005), 283–298.
- [20] H.-K. Choi, S.-K. Park and J.-W. Ra, Reconstruction of a high-contrast penetrable object in pulsed time domain by using the genetic algorithm, *IEEE International Sym. On Geoscience and Remote Sensing* **1** (1997), 136–138.

- [21] M.W. Chevalier, R.J. Luebbers and V.P. Cable, FDTD local grid with material traverse, *IEEE Trans Antennas and Propagation* **45**(3), March 1997.
- [22] C. de Boor, *A Practical Guide to Splines*, Springer-Verlag, New York, 1978.
- [23] W. Chien and C.C. Chiu, Using NU-SSGA to reduce the searching time in inverse problem of a buried metallic object, *IEEE Transactions on Antennas and Propagation* **53**(10) (October 2005), 3128–3134.
- [24] C.-L. Li, C.-W. Liu and S.-H. Chen, Optimization of a PML absorber's conductivity profile using FDTD, *Microwave and Optical Technology Letter* **37** (2003), 380–383.

Copyright of International Journal of Applied Electromagnetics & Mechanics is the property of IOS Press and its content may not be copied or emailed to multiple sites or posted to a listserv without the copyright holder's express written permission. However, users may print, download, or email articles for individual use.